引用格式：ZHANG Qi-hao, ZHANG Ling-xuan, LI Zhong-yu, *et al*. Antenna Array Initial Condition Calibration Method for Integrated Optical Phased Array[J]. *Acta Photonica Sinica*, 2020, **49**(7):0726001
张其浩,章羚旋,李中宇,等.用于光学相控阵天线的初始校准算法[J].光子学报,2020,**49**(7):0726001

用于光学相控阵天线的初始校准算法

张其浩[1,2],章羚旋[1],李中宇[1],吴伟[1,2],王国玺[1,2],孙笑晨[1,2],赵卫[1,2],
张文富[1,2]

(1 中国科学院西安光学精密机械研究所 瞬态光学与光子技术国家重点实验室,西安 710119)
(2 中国科学院大学,北京 100049)

摘 要:针对光学相控阵存在难以校准的相位误差的问题,改进了旋转电矢量相控阵天线初始相位校准方法.与原始方法相比,该方法改变了相位计算方法,并且每测算出一个单元的相位误差立即进行相位矫正,然后测算并矫正下一个单元的相位误差,避免了原始方法在初始相位误差分布范围较广且光功率测量精度有限的情况下可能出现的π相位错误.仿真结果表明,原始方法校准后主瓣光强的平均值最多达到理想值的70.8%,标准差至少为19.1%;而改进方法校准后的主瓣强度均值至少可以达到理想值的87.6%,标准差最大7.3%,证明了改进方法具有更高的统计精度和可预测性.制备了9×9光学相控阵芯片,芯片初始的栅瓣抑制比为2.12 dB,改进的旋转电矢量法校准后则达到了4.68 dB,证明了该方法的有效性与实际应用价值.

关键词:集成芯片;数值模拟;相控阵;天线方向图;相位校准;误差分析
中图分类号:O439 **文献标识码**:A **doi**:10.3788/gzxb20204907.0726001

Antenna Array Initial Condition Calibration Method for Integrated Optical Phased Array

ZHANG Qi-hao[1,2], ZHANG Ling-xuan[1], LI Zhong-yu[1], WU Wei[1,2], WANG Guo-xi[1,2], SUN Xiao-chen[1,2], ZHAO Wei[1,2], ZHANG Wen-fu[1,2]

(1 *State Key Laboratory of Transient Optics and Photonics, Xi'an Institute of Optics and Precision Mechanics, Chinese Academy of Science, Xi'an* 710119, *China*)
(2 *University of Chinese Academy of Sciences, Beijing* 100049, *China*)

Abstract: To solve the problem that the phase error of the optical phased array is difficult to calibrate, rotating element electric field vector calibration method is modified. Comparing with the traditional method, the new method modifies the algorithm and corrects the phase immediately after measuring the phase error of one unit, then measures and corrects the phase of the next unit. Possible π phase error in traditional method is avoided when large initial phase distribution and finite optical power measurement accuracy present. The simulation results show that the main lobe intensity calibrated with the original method reaches at most 70.8% of the ideal value on average, and the standard deviation is at least 19.1%.

Foundation item: The National Natural Science Foundation of China (Nos. 61675231, 61635013, 61705257, 61805277), the Strategic Priority Research Program of the Chinese Academy of Sciences (No. XDB24030600), the Youth Innovation Promotion Association of Chinese Academy of Sciences (No. 2016353).

First author: ZHANG Qi-hao (1994—), male, M. S. degree candidate, mainly focuses on integrated photonics devices. Email: zhangqihao2016@opt.cn
Supervisor (Contact author): ZHANG Wen-fu (1982—), male, professor, Ph. D. degree, mainly focuses on integrated photonics & nanophotonics. Email: wfuzhang@opt.ac.cn

Received: Sept.19,2019; **Accepted**: May 13,2020

While after calibration with the modified method the main lobe intensity reaches at least 87.6% of the ideal value on average, the maximum standard deviation is 7.3%. The modified method produces statistically more accurate and predictable calibration result. A 9×9 optical phased array chip is manufactured. The initial grating lobe suppression ratio ofthe chip is 2.12 dB. Calibrated with this modified method the ratio reaches 4.68 dB. The effectiveness and practical application value of this method are proved.

Key words: Integrated chips; Numerical calculation; Phased array; Antenna patterns(antenna); Phase calibration; Error analysis

OCIS Codes: 260.2110; 280.5110; 120.5050; 010.3640; 130.3120

0 Introduction

A variety of optical sensor technologies have been widely demanded and successfully adopted in modern electronic products from smartphones to autonomous driving systems. Optical Phased Array (Optical phased array, OPA) is one of the optical technologies that frequently comes under the spotlight lately for its potential use in autonomous vehicle and 3D sensing applications. OPA uses an array of optical antennas which can be individually addressed for phase (and sometimes amplitude) tuning in order to form a beam of light and to steer the beam to desired directions. Compared to radio frequency phased array that has been extensively used in many long distance ranging applications, optical phased array hasn't seen wide adoption partly due to the practical difficulty to pack a large number of individual optical antennas (and corresponding phase tuning elements) at distances comparable to optical wavelength. With the rise of integrated photonics, Si photonics in particular, people find ways to integrate many diffraction-limited optical elements close to each other at large scale by low-cost semiconductor wafer level process[1-3]. Si photonics-based integrated OPA quickly becomes a hot topic in both academic research[4-7] and entrepreneurial endeavors.

Integrated OPA is in its infancy for practical applications and many engineering challenges limiting its performance and practicality await for better solutions. One such challenge is to calibrate the almost random phase error (and to a lesser extend the amplitude error) among an array of waveguide-distributed antennas due to unavoidable processing errors (such as line edge roughness and lithography errors). Even very small width variations that modern semiconductor processes provide can cause large phase error and chaotic far-field patterns when such variations are accumulated throughout millimeter long waveguide routes which are required for even moderate number of antennas. Therefore, calibrating initial phase condition of an antenna array is required for every and each OPA product and the effectiveness and efficiency of the calibration is a key to successful commercialization.

Some mature calibration methods have used in radio frequency phased array. Such as near-field method[8] requires measuring single antenna near-field data is not practical for OPA due to its micrometer size antenna. And the mutual coupling method[9] requires a single antenna transmits signals and another antenna to receive. However the integrated OPA generally does not have single antenna transmission and reception function. Phase toggling method[10] demands large and fine far field pattern measurement which makes corresponding optical calibration system complex and compute-intensive. None of these three calibration methods are suitable for integrated OPA.

Some generic optimization methods such as hill climbing, genetic algorithm, particle swam optimization, stochastic gradient descent algorithm and etc.[11-14] can provide fairly good calibration in some cases. However all smart algorithms generally cannot avoid local extremum uncertainty (which is a severe issue for most OPA with larger-than-wavelength-spaced antennas) and are not scaled well with the size of the antenna array.

Rotating element Electric field Vector (REV) method[15-16] is a more efficient far-field method while suffers possible π phase error when initial phases span the whole 2π space (which is common for optical band while less common in microwave band) at finite optical power measurement accuracy.

This paper propose a modified REV method that avoids the possible π phase error in traditional REV. The improvement in modified REV method has great implications in practical deployment of OPA products. This modified REV method is applied to a 9×9 OPA with unevenly spaced antenna array (for better side lobe suppression) and show that it produces statistically more accurate, predictable and converged calibration result.

1 Theory

1.1 Modified REV

Rotating element electric field vector method calculates the initial phases of each antenna by finding the maximum and minimum optical power at a fixed single far-field point while varying the phase of each antenna from 0 to 2π. For each antenna, from the measured phase shift $\Delta\varphi$ from the initial state to the maximum power state, the corresponding maximum power and the minimum power values, the phase shift from its initial state to the calibrated state (i.e. an ideal phase distribution for all antennas to maximize the power at the given far field point) of this antenna is calculated. Reset this antenna to its initial phase and repeat this process for the next antenna till the phase shift of all antennas is determined and the OPA is considered calibrated. The phase shift calculation in this method is correct in theory however in practice, as explained later, can produce π phase uncertainty error due to wide initial error range (0~2π) and finite optical power measurement accuracy.

Instead, modified REV method lets $\Delta\varphi$ as the phase shift from the initial state to the calibrated state and set the antenna to this maximum power phase when repeating the same calibration step on the next antenna. This process quickly converges and approaches to the ideal calibration condition with the number of calibrated antennas. And this simple approach avoids π phase uncertainty and do not rely on precise maximum and minimum power measurement data. The calibration process is shown in Fig. 1 and the theory is explained in details below.

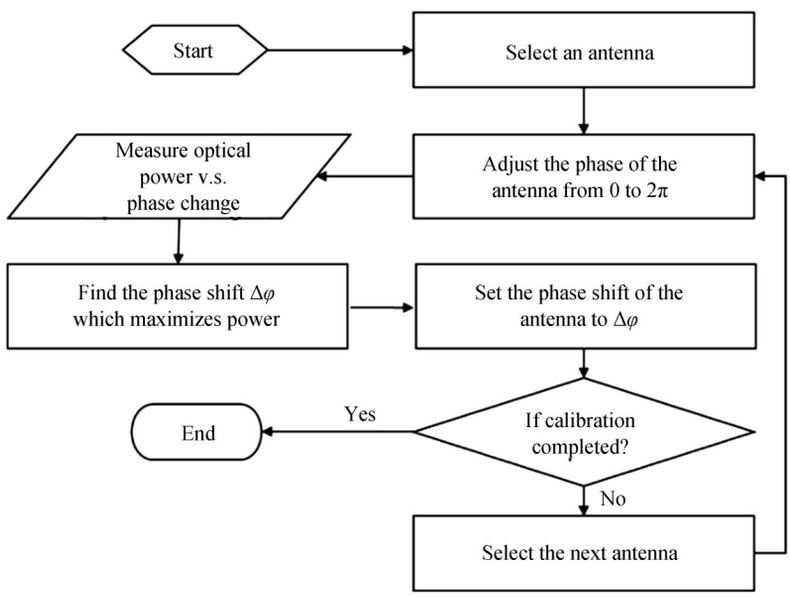

Fig. 1 Phase calibration flow of the presented modified REV method

The electric field of the nth antenna at a fixed far-field point Q is

$$\boldsymbol{E}_n = A_n(\alpha, \beta, r)\exp\left(\mathrm{i}\omega t - \mathrm{i}\boldsymbol{k}_n \cdot \boldsymbol{r}_n + \mathrm{i}\varphi_n\right)\cdot \boldsymbol{e} \tag{1}$$

where α, β and r is the coordinates of point Q in polar coordinate system, $A_n(\alpha, \beta, r)$ is the amplitude of the antenna, ω is the optical frequency, $\boldsymbol{r}_n$ is the distance vector from the antenna to the point Q, φ_n is the initial phase of the antenna, and $\boldsymbol{e}$ is unit vector determined by polarization.

In practice the interested far field target is significantly farther in distance than the size of the OPA thus the directions of electric field and distance vectors of all antennas can be approximately considered the same. In addition, as all antennas share a single coherent light source the polarization of every antenna is the same. Eq. (1) can then be simplified to scalar form. The total electric field at point Q is

$$E_0 = \sum_{n=1}^{N} A_n \exp\left(\mathrm{i}\omega t - \mathrm{i}kr_n + \mathrm{i}\varphi_n\right) = \exp(\mathrm{i}\omega t)\sum_{n=1}^{N} A_n \exp\left(\mathrm{i}\phi_n\right) \tag{2}$$

where $\phi_n = \varphi_n - kr_n$ is the phase of the nth antenna at point Q. The intensity is

$$I_0 = \left|E_0\right|^2 = \left|\exp(\mathrm{i}\omega t)\right|^2 \cdot \left|\sum_{n=1}^{N} A_n \exp(\mathrm{i}\phi_n)\right|^2 = \left|\sum_{n=1}^{N} A_n \exp(\mathrm{i}\phi_n)\right|^2 \tag{3}$$

When the phase of the mth antenna is changed by $\Delta\varphi$, the intensity becomes

$$I(\Delta\varphi) = \left|\sum_{n=1}^{N} A_n \exp(\mathrm{i}\phi_n) - A_m \exp(\mathrm{i}\phi_m) + A_m \exp(\mathrm{i}\phi_m + \mathrm{i}\Delta\varphi)\right|^2 \tag{4}$$

Define

$$E_{-m} = \sum_{n=1}^{N} A_n \exp(\mathrm{i}\phi_n) - A_m \exp(\mathrm{i}\phi_m) = A_{-m} \exp(\mathrm{i}\phi_{-m}) = v_m + \mathrm{i}w_m \tag{5}$$

where E_{-m} represents the sum of the electric fields of all antennas except the mth, A_{-m} is the amplitude of E_{-m}, and v_m and w_m are the real and imaginary part of the E_{-m}, respectively.

The intensity $I(\Delta\varphi)$ can then be expressed as

$$I(\Delta\varphi) = v_m^2 + w_m^2 + A_m^2 + 2v_m A_m \cos(\phi_m + \Delta\varphi) + 2w_m A_m \sin(\phi_m + \Delta\varphi) \tag{6}$$

A derivative calculation shows the following condition must be met at an extremum of $I(\Delta\varphi)$

$$\Delta\varphi + \phi_m = \begin{cases} \arctan(w_m/v_m) \\ \pi + \arctan(w_m/v_m) \end{cases} \tag{7}$$

The intensity at Q reaches its maximum when $\Delta\varphi + \phi_m = \arctan(w_m/v_m)$as shown by the second derivative of $I(\Delta\varphi)$ without losing generality by assuming $A_m > 0$

$$\left.\frac{\mathrm{d}^2 I}{(\mathrm{d}\Delta\varphi)^2}\right|_{\Delta\varphi = \arctan\frac{w_m}{v_m} - \phi_m} = -2A_m\sqrt{v_m^2 + w_m^2} < 0 \tag{8}$$

and the maximum intensity $I_{\max}$ is

$$I_{\max} = I\left(\arctan\frac{w_m}{v_m} - \phi_m\right) = \left(\sqrt{v_m^2 + w_m^2} + A_m\right)^2 = \left(\left|E_{-m}\right| + \left|E_m\right|\right)^2 \tag{9}$$

It simply implies that the intensity of point Q reaches its maximum with the mth antenna and the combined field of the rest of the antennas are in-phase. This simple principle guides the whole calibration process. After the $\Delta\varphi$ of each antenna is obtained by varying its phase till maximum measured optical power at Q, the antenna is fixed at this phase and the next antenna is calibrated to the next maximum intensity condition. Repeat this process until all antennas are calibrated and set to their maximum intensity phase. The principle also guarantees the monotonic increase of the measurement optical power which helps reduce any possible ambiguity during the process. This method can be used for calibrating an OPA antenna array distributed in any patterns and does not demand any particular order in selecting antennas.

The whole process may be explained more intuitively in Fig. 2 (a)～(f). The related electrical field is drawn in a vector plane where the length and the angle from x-axis of a field represent its absolute amplitude and phase respectively. The following text refer to a field vector in this representation as opposed to a real space representation.

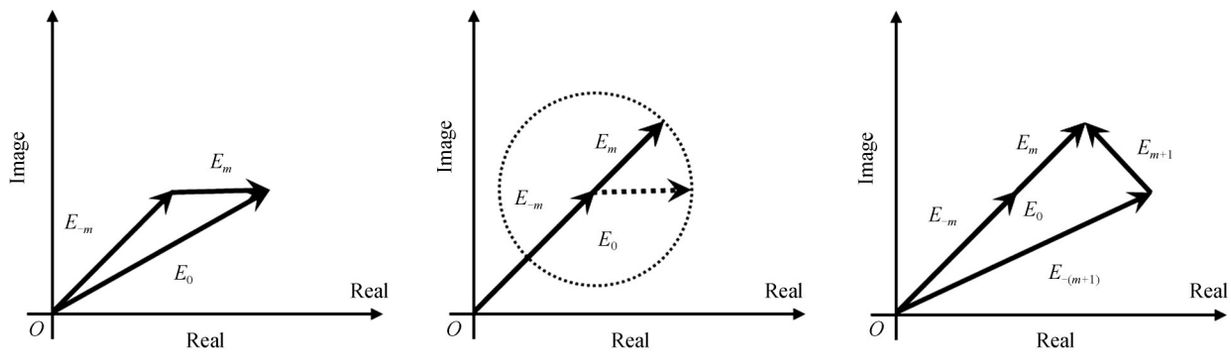

(a) Electrical vector before E_m is calibrated (b) Electrical vector after E_m is calibrated (c) Keeping E_m at this phase

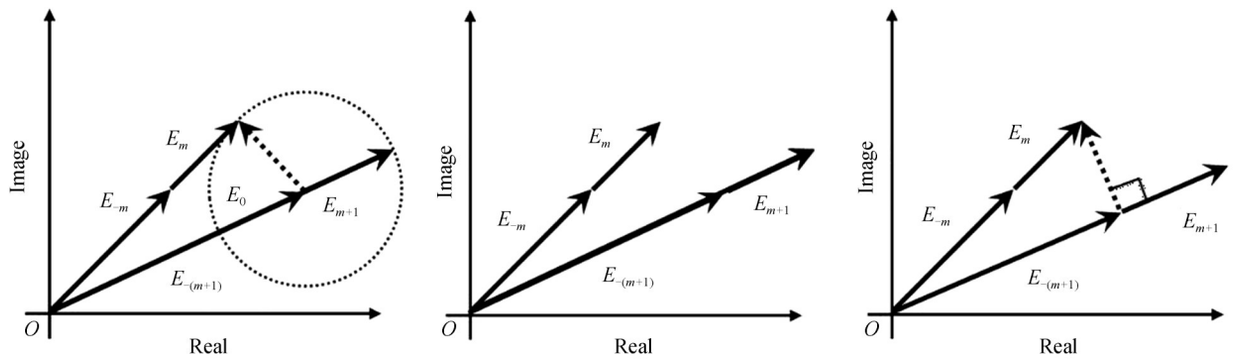

(d) Electrical vector after E_{m+1} is calibrated

(e) The difference between calibrated E_m and E_{m+1}

(f) A particular case where the phase change of E_{m+1} is π/2

Fig. 2 Schematic diagram of electrical vector changes during modified REV method.

In practice when measurement error inevitably present, the final antenna array phase condition as well as the maximum intensity at Q may still be slightly off from their ideal values, even so, the following analysis shows the calibration well approaches the ideal condition, traditional REV also presents similarly if not worse results. In practice, the calibration process in production demands a statistically predictable and converged result.

1.2 Error analysis

For practical considerations, the errors need be analyzed in this method. It can be seen that the calibrated field vectors of the mth and the $(m+1)$th antennas that are aligned to E_{-m} and $E_{-(m+1)}$, respectively, as shown in Fig. 2(e) are generally not aligned with each other. Therefore at least one of the calibrated phase values of mth and $(m+1)$ th antennas differs from its ideal value and it represents an intrinsic error of the method. However, as explained, such error does not pose significant overall calibration error and the error is more limited or converged than that in traditional REV method when measurement errors exist.

As shown in Fig.2(f), the relative intrinsic phase error of a certain antenna $(m+1)$ reaches its maximum in this case and the error, the phase difference between the $(m+1)$th and the mth antenna, in general satisfies

$$\delta\varphi_{m+1} \leqslant \arcsin\frac{|A_{m+1}|}{|E_0|} \tag{10}$$

where $A_{(m+1)}$ is the amplitude of the $(m+1)$ th antenna; E_0 is the combined electric field at point Q before calibrating the $(m+1)$th antenna. It implies $\delta\varphi_{(m+1)}$ continues to decrease with the increase of the number of the calibrated antennas as $|E_0|$ becomes larger when more antenna field vectors getting approximately aligned.

For example, after the first antenna is calibrated, $|E_0| \geqslant A_1 \cong A_2$, the phase difference between the second and the first antenna

$$\delta\varphi_2 \leqslant \arcsin\frac{A_2}{|E_0|} \leqslant \pi/2 \tag{11}$$

while for the third antenna to the calibrated, $|E_0| \geqslant \sqrt{2}\,A_3$, the phase difference

$$\delta\varphi_3 \leqslant \arcsin\frac{A_3}{|E_0|} \leqslant \pi/4 \tag{12}$$

and it can be easily seen that $\delta\varphi$ continues to reduce as more antennas are calibrated.

In an OPA where the phase error is mostly introduced by waveguide size variations, antennas initial phases tend to be widely distributed thus the intrinsic phase error after calibration also randomly distributes within $\pm\delta\varphi$ and the calibration imperfection caused by such distributed error is generally far less severe than the worst case scenario. In addition, if higher calibration accuracy is required, the same process can be repeated. And since $|E_0|$ becomes significantly larger after the first calibration process the intrinsic error becomes even smaller. Furthermore it is generally sufficient to only perform the second calibration on first few antennas whose phase errors are relatively larger than others.

Another type of error rises from errors in measurement (mainly measured optical power) and in

calculations using the measurement data (phase change between initial to maximum power conditions). In traditional REV, such measurement error becomes more severe due to the way of calculating phase values that can introduce possible π phase error. The equation to calculate the initial phase of an antenna in traditional REV method is

$$\phi_e = \arctan\left[\sin\left(\Delta\varphi_{pmax}\right)\Big/\left(\cos\left(\Delta\varphi_{pmax}\right)+\frac{\sqrt{p_{max}/p_{min}}-1}{\sqrt{p_{max}/p_{min}}+1}\right)\right] \tag{13}$$

where $\Delta\varphi_{pmax}$ is the phase shift from the initial state to the maximum power state; p_{max} and p_{min} are the maximum and minimum power at point Q, respectively.

The arctan function produces a value between $[-\pi/2, \pi/2]$ while the possible true phase difference ranges a whole 2π. It requires the algorithm to decide whether or not to purposely add a π to its solution based on the value of $\Delta\varphi_{pmax}$. Such decision in principle has no problem, however, it presents possible error when the phase change from its initial value to the measured maximum power point occurs close to $\pm\pi/2$ at which small optical power error may produce completely wrong determination.

As shown in the second section, even a 0.1% intensity error can cause poor calibration results. In a microwave radar, where the initial phase shifts of antennas are generally not as widely diverged as in an OPA, such issue is not as severe. Such practically inevitable error is considered in the second section and its effect between traditional REV and modified REV methods is compared.

2 Simulation

2.1 Description

To test modified REV calibration method, the following simulation work is performed with a 9×9 two-dimensional optical phased array operating at 1 550 nm wavelength. Assuming all antennas share the same emission profile including intensity and far-field distribution, the optical power non-uniformity introduced by some Si photonics integrated OPA designs (e.g. power splitting[17-18] or cascaded power tapping[19-20]) has tolerable detrimental effect.

To simulate a real-world process of finding the maximum optical power at Q and calculating the phase shift, the phase can only be varied in a finite step provided by the resolution of a digit-to-analog converter (Digit-to-Analog Converter, DAC). Considering a DAC resolution ranges from 3-bit to 8-bit (for $0\sim2\pi$ range), its effect is tested on calibration result.

A small Gaussian-distributed error is introduced to the far field optical power measurement data. In practice, this error rises from multiple sources including IR camera measurement inaccuracy, side lobe light scattered by a test system, scattered light from chip-coupled light source, stray ambient light, etc. The Gaussian error is within ±0.1% (at 3σ) of the peak far field intensity. However it has a non-negligible effect on calibration result.

2.2 Results and analysis

First, the far field of the OPA is calculated with ideal initial phase condition, i.e. phases are equal for all antennas as shown in Fig. 3(b) and the result is shown in Fig.3(a). The far field are the intensity values at the spherical surface originated from the OPA ($x=0$, $y=0$) with a radius of 1 m and (φ, θ) represent the angles from z-axis in $x-z$ and $y-z$ planes respectively. A special case with intensity vs. θ at $\varphi=0$ shows one of the directions with the worst side lobe suppression which generally limits this OPA system to about 60^0 Field of View (FOV). A typical far-field, antennas phase map, and far-field intensity with θ at $\varphi=0$ with randomly distributed initial phase between 0 and 2π are shown Fig.3(d)~(f) respectively. The far field intensity is scaled with the same range as in the ideal case. It can be easily seen that a widely distributed initial phase errors generally destroy constructive interference and result in chaotic far field and much lower peak values. The same three plots after the initial phase errors are calibrated by modified REV method are shown in Fig.3 (g)~(i). The calibration is processed in one pass with 8-bit phase tuning resolution and Gaussian intensity error as mentioned earlier. It can be seen that the calibrated results agree very well with the ideal phase condition results and the system is considered to be calibrated (although the initial phases at some antennas may be off from their

ideal values).

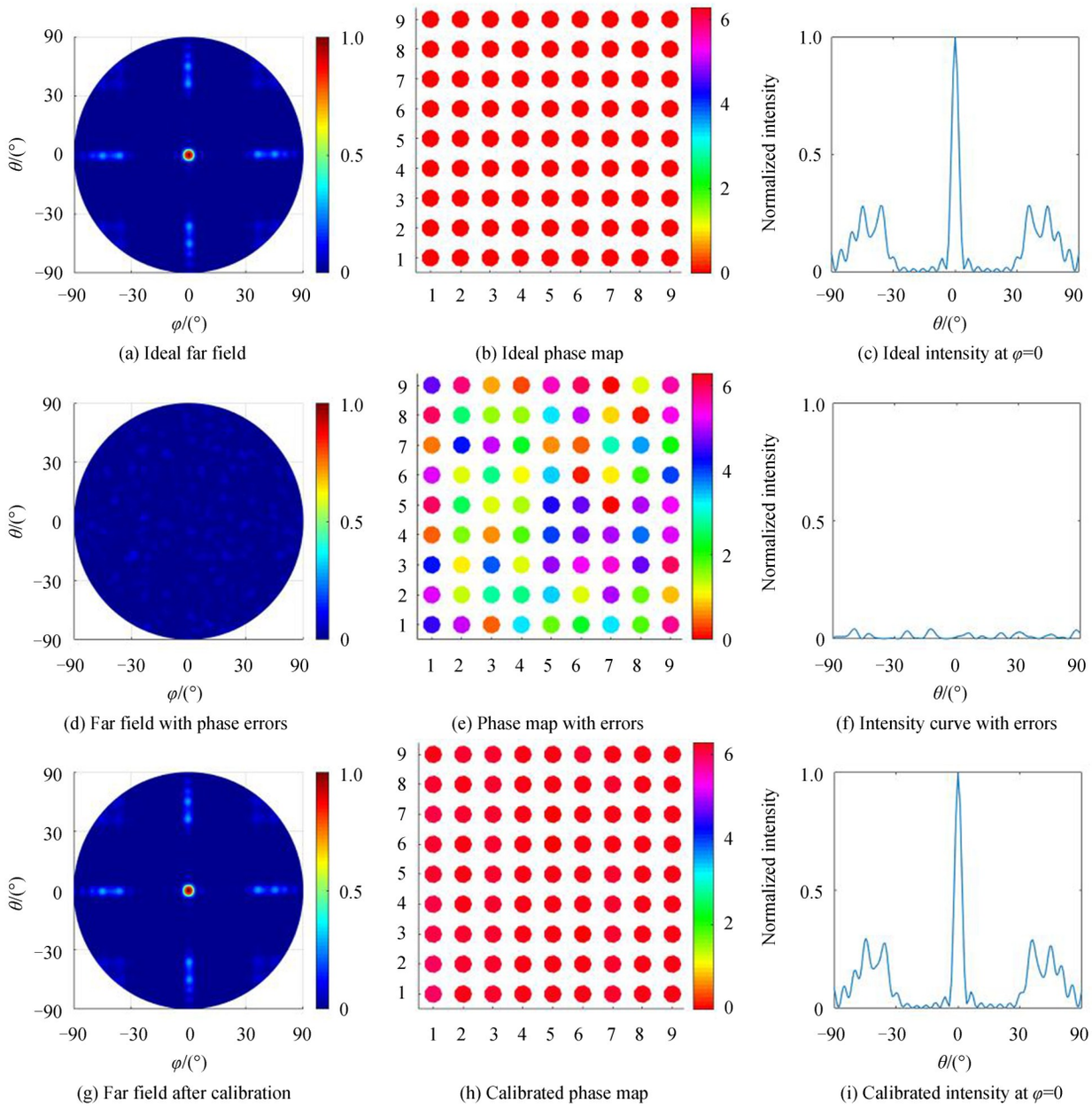

Fig. 3 The simulation results of far field.

The 1D far field in Fig.3 (c) may be easily use as a visual benchmark to compare calibration results among cases while it is more convenient to use the relative intensity, i.e. scaled with the same range as the ideal case, at Q ($\theta=0$, $\varphi=0$) as a figure-of-merit to quantitatively compare the statistical calibration performance by different methods at different conditions. It is also called as calibrated intensity in following texts.

To compare the calibration performance between modified REV (mREV) and traditional REV as well as to test the effect on phase tuning resolution, calibration process is performed by both mREV and REV for 1 000 cases of randomly generated (within $0\sim2\pi$) initial phase maps with phase tuning resolutions ranging from 3-bit to 8-bit. The results are summarized in Fig.4 (a). It can be seen that at any phase tuning resolution the overall calibration performance of mREV is much better than REV in terms of the average calibrated intensity and its error (i.e. root-mean-square error). To show how the calibrated intensity statistically distributes, the 6-bit phase resolution case is picked and plot the probability distribution of calibrated intensity of the 1 000 cases processed by mREV and REV, respectively, in Fig.4(b). It clearly shows that the calibrated intensity of REV

is less accurate and more diverged than that of mREV. In practice, it's obviously preferred to have a robust product calibration process with results produced by mREV.

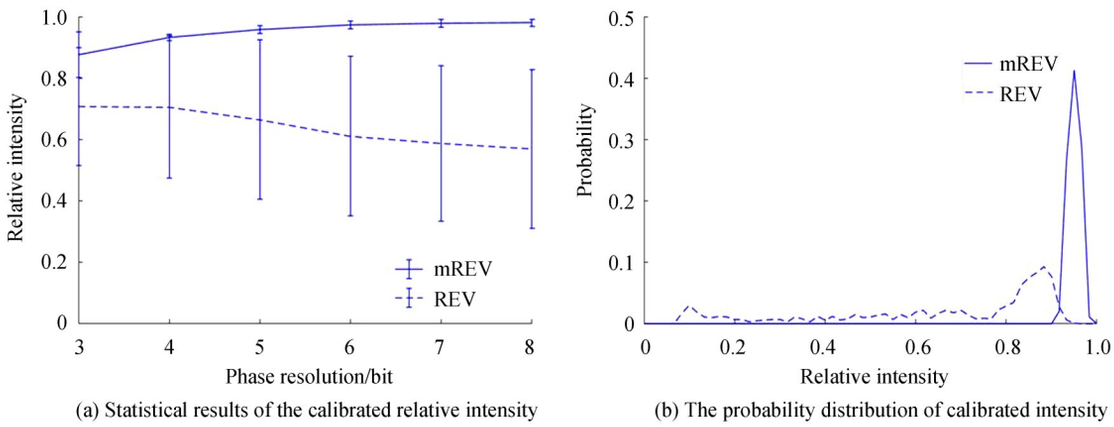

(a) Statistical results of the calibrated relative intensity (b) The probability distribution of calibrated intensity

Fig. 4 The statistical results of calibrated main lobe

For mREV, the increase of average calibrated intensity with phase tuning resolution, i.e. number of bits, is easy to understand as the accuracy of $\Delta\varphi$ for each antenna increases. The same analysis doesn't apply to the REV cases as shown in Fig.4 (a) where the average calibrated intensity is slightly higher at lower resolution while the maximally achieved calibrated intensity (upper boundary) presents at medium resolutions. As already known for REV, another source of error, π phase error in certain initial phase conditions, sometimes determines overall calibration performance. At low resolution, i.e. smaller bits, although the phase accuracy is low, the chance to make a π error is also low as the intensity difference between two adjacent phase tuning steps is often too large to produce incorrect determination even with the presence of power measurement errors.

The above analysis explains the histograms of the calibrated antennas phases. Some typical histograms are shown in Fig.5. The calibrated phases are generally more concentrated within a narrow range in mREV cases. While in cases calibrated by traditional REV, although phases of many antennas are also within a similar narrow range there are always certain phases located in another π-shifted range and such errors cause poor calibration

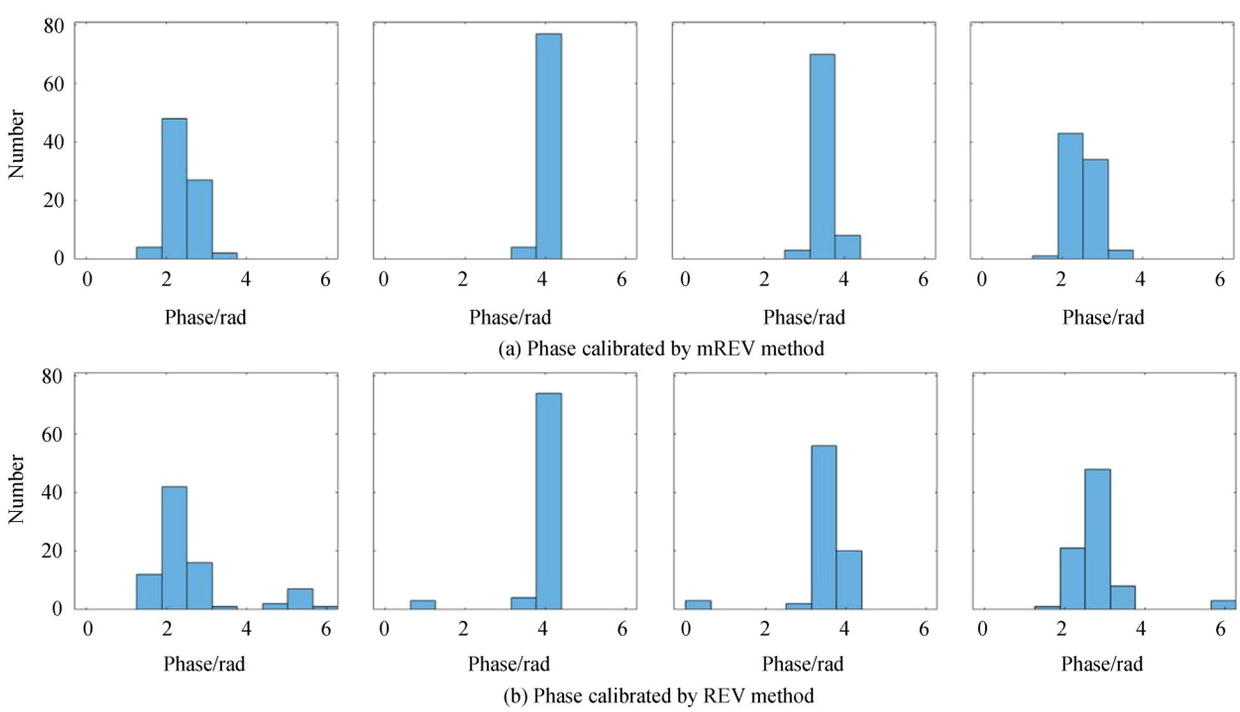

(a) Phase calibrated by mREV method

(b) Phase calibrated by REV method

Fig. 5 Histograms of the calibrated antennas phases in four typical cases

result.

3 Experiment

For experimentally validating the simulation results, a 9×9 two-dimensional optical phased array device is calibrated, as shown in Fig.6(a). The OPA device is designed as a non-uniform antenna array and fabricated with silicon photonics technology. This device has 81 thermal phase shifters and each of them is independently adjustable. A 1 310 nm laser is coupled into the OPA chip through a polarization controller and a grating coupler. A computer, adjustable DC voltage-stabilized power supply and 81-channel digital-to-analog converter are used to control the voltage applied to each antenna unit. Applying a series different voltages on a phase shifter, the phase of the optical emission from the antenna unit is tuned from 0 to 2π. Then, a series different far field images are collected by a high numerical aperture (NA=0.5) lens and captured with InGaAs infrared camera (256×320 pixels), as shown in Fig.6(b).

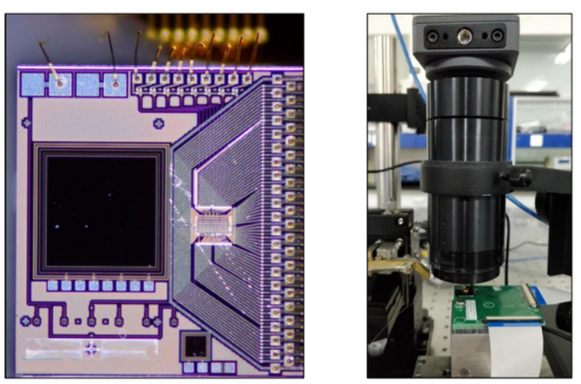

(a) Chip photo (b) Lens and camera photo

Fig. 6 Experiment installation

Using mREV method to calibrate the device, computer program automatically searches what voltage make the far field pattern closest to the target pattern, then applies the voltage on the phase shifter. Repeating this process on all phase shifters, the calibration experiment is finished. The whole calibration process is easy to operate, just input the voltage sweep range, step length and sequence of phase shifters, the program will complete the calibration.

The initial grating lobe suppression ratio of this OPA device is 2.12 dB, as shown in Fig.7 (a)~(c). After calibration with mREV method, the grating lobe suppression ratio achieves 4.68 dB, as shown in Fig.7 (d)~(f). Comparing with the initial far-field pattern, in the calibrated pattern more energy is concentrated on the main lobe, meanwhile the grating lobe is weakened a lot. Although the grating lobe suppression ratio doesn't reach the design value (6 dB), it is not because of the mREV method but because of on-chip thermal crosstalk and manufacturing errors.

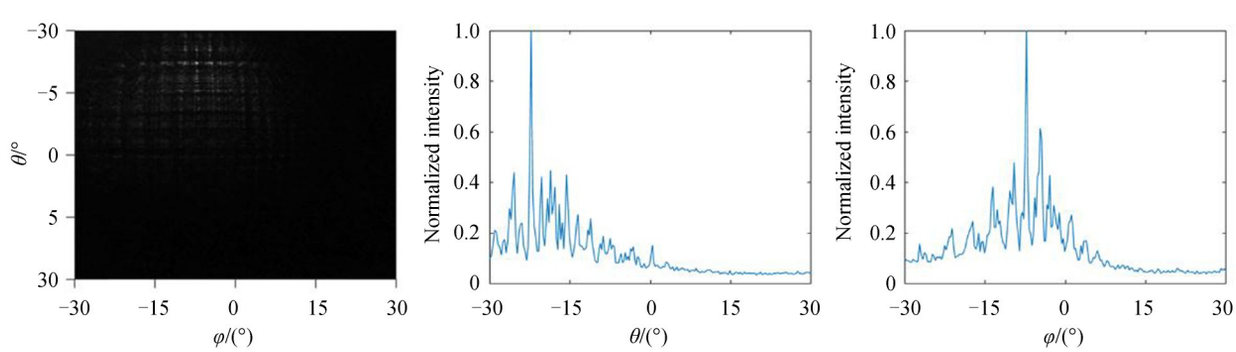

(a) Initial far-field image (b) Initial intensity curves (θ) (c) Initial intensity curves (φ)

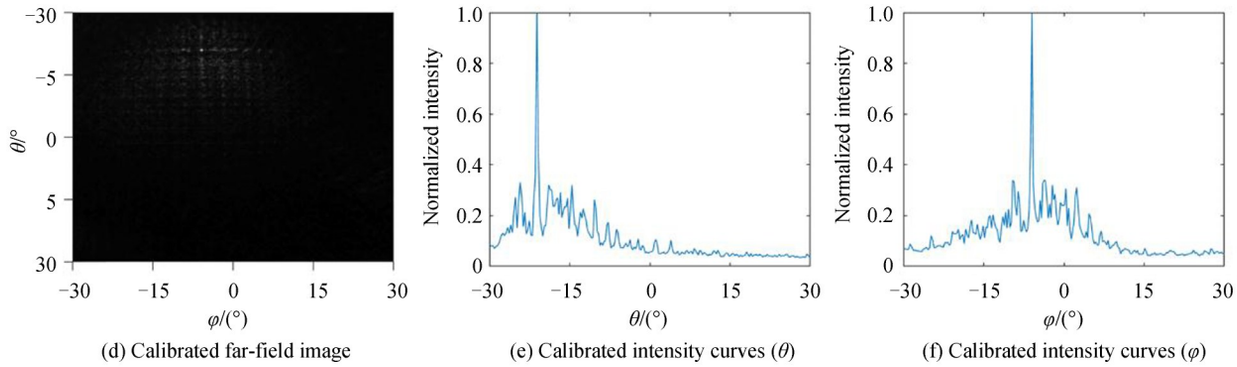

(d) Calibrated far-field image (e) Calibrated intensity curves (θ) (f) Calibrated intensity curves (φ)

Fig. 7 The experimental far field

4 Conclusion

The paper presents a modified rotating element electric field vector method for calibrating the antenna array initial condition of an optical phased array with arbitrary initial phase distribution, the number of antennas and the arrangement of the antennas. The numerical simulation results show that the method can calibrate ideal far-field intensity distribution to practically sufficient accuracy. Even with the presence of significant random measurement errors representing realistic situations in practice, the main lobe intensity can statistically reach more than 90% of the ideal case. In addition, the results show a much less scattered error range, which is essential for calibration in practical deployment, compared to the results by traditional REV at the same simulated realistic conditions. The improvement in both accuracy and precision of the initial phase condition calibration by the modified REV results from the absence of π-shift ambiguity which is inevitable, but less severe in radio frequency phased array applications, in the traditional REV method. Due to the improved accuracy, precision and stability, the presented modified REV method provides great benefits in practice when calibrating OPA products with large number of antennae and phase shifters such as those are made by integrated photonics. The complexity in calibration and testing is currently one of the obstacles to accelerate the deployment and mass production of OPA devices, and the modified REV method can help make the progress. The experiment proves part of the simulation results, in future, more OPA devices should be calibrated to prove all of the simulation results.

References

[1] SUN Jie, TIMURDOGAN E, YAACOBI A, *et al*. Large-scale nanophotonic phased array [J]. *Nature*, 2013, **493**(7431):195-199.

[2] YANG Wei-jian, SUN Tian-bo, RAO Yi, *et al*. High speed optical phased array using high contrast grating all-pass filters [J]. *Optics Express*, 2014, **22**(17):20038-20044.

[3] HULME J C, DOYLEND J K, HECK M J R, *et al*. Fully integrated hybrid silicon two dimensional beam scanner[J]. *Optics Express*, 2015, **23**(5):5861-5874.

[4] RAVAL M, POULTON C V, WATTS M. Unidirectional waveguide grating antennas for nanophotonic phased arrays [C]. Conference on Lasers and Electro-Optics, 2017:STh1M.5.

[5] CHUNG S W, ABEDIASL H, HASHEMI H. A monolithically integrated large-scale optical phased array in silicon-on-insulator CMOS[J]. *IEEE Journal of Solid-State Circuits*, 2018, **53**(1), 275-296.

[6] KANG G, KIM S, YOU J, *et al*. Silicon-based optical phased array using electro-optic p-i-n phase shifters[J]. *IEEE Photonics Technology Letters*, 2019, **31**(21): 1685-1688.

[7] MILLER S A, CHANG Y C, PHARE C T, *et al*. Large-scale optical phased array using a low-power multi-pass silicon photonic platform[J]. *Optica*, 2020, **7**(1): 3-6.

[8] PATTON W T, YORINKS L H. Near-field alignment of phased-array antennas[J]. *IEEE Transactions on Antennas and Propagation*, 1999, **47**(3):584-591.

[9] AUMANN H M, FENN A J, WILLWERTH F G. Phased array antenna calibration and pattern prediction using mutual coupling measurements[J]. *IEEE Transactions on Antennas and Propagation*, 1989, **37**(7):844-850.

[10] LEE K M, CHU R S, LIU S C. A built-in performance-monitoring/fault isolation and correction (PM/FIC) system for active phased-array antennas[J]. *IEEE Transactions on Antennas and Propagation*, 1993, **41**(11):1530-1540.

[11] HUTCHISON D N, SUN Jie, DOYLEND J K, *et al*. High-resolution aliasing-free optical beam steering[J]. *Optica*,

2016, **3**(8):887-890.

[12] SON S H, EOM S Y, JEON S I, *et al*. Automatic phase correction of phased array antennas by a genetic algorithm[J]. *IEEE Transactions on Antennas and Propagation*, 2008, **56**(8):2751-2754.

[13] KOMLJENOVIC T, PINTUS P. On-chip calibration and control of optical phased arrays [J]. *Optics Express*, 2018, **26**(3):3199-3210.

[14] KWONG D, HOSSEINI A, COVEY J, *et al*. On-chip silicon optical phased array for two-dimensional beam steering [J]. *Optics Letters*, 2014, **39**(4):941-944.

[15] TAKAHASHI T, MIYASHITA H, KONISHI Y, *et al*. Theoretical study on measurement accuracy of rotating element electric field vector (REV) method[J]. *Electronics and Communications in Japan*, 2006, **89**(1), 22-33.

[16] MANO S, KATAGI T. A method for measuring amplitude and phase of each radiating element of a phased array antenna [J]. *Electronics and Communications in Japan* (*Part I: Communications*), 1982, **65**(5):58-64.

[17] ASHRAFI NIA B, YOUSEFI L, SHAHABADI M. Integrated optical phased array nano-antenna system using a plasmonic rotman lens[J]. *Journal of Lightwave Technology*, 2016, **34**(9):2118-2126.

[18] IM C S, BHANDARI B, LEE K P, *et al*. Silicon nitride optical phased array based on a grating antenna enabling wavelength-tuned beam steering[J]. *Optics Express*, 2020, **28**(3):3270-3279.

[19] HASHEMI H. Large-scale monolithic optical phased arrays [C]. Optical Fiber Communication Conference, 2019: Tu3E.5.

[20] SUN Jie, HOSSEINI E S, YAACOBI A, *et al*. Two-dimensional apodized silicon photonic phased arrays [J]. *Optics Letters*, 2014, **39**(2):367-370.